Petroleum Science 19 (2022) 245–253

Contents lists available at ScienceDirect

Petroleum Science

journal homepage: www.keaipublishing.com/en/journals/petroleum-science

Original Paper

Self-healing elastomer modified proppants for proppant flowback control in hydraulic fracturing

Jian-Da Li, Gui-Cai Zhang*, Ji-Jiang Ge, Wen-Li Qiao, Ping Jiang, Hai-Hua Pei

School of Petroleum Engineering, China University of Petroleum (East China), Qingdao, 266580, Shandong, PR China

ARTICLE INFO

Article history:
Received 30 March 2021
Accepted 8 December 2021
Available online 31 December 2021

Edited by Yan-Hua Sun

Keywords:
Proppant flowback
Self-healing elastomer
Self-aggregation
Adhesion force

ABSTRACT

To address proppant flowback issues during post-fracturing treatments and production, self-healing elastomer modified proppants (SMPs) are proposed. Owing to their inherent self-aggregation behavior, the SMPs can aggregate together spontaneously to prevent proppant flowback and increase the pack porosity. It is noteworthy that the SMPs have a firm and dry self-healing elastomer (SE) coating, making their storage, transport and use as conventional proppants possible. The SE synthesized through polymerization is rich in amidogens and carbonyl groups as characterized by Fourier transform infrared spectroscopy and the proton nuclear magnetic resonance. Thermal and thermomechanical properties of the SE coating are revealed by the thermogravimetric analysis, the differential scanning calorimetry and the rheological tests. The self-aggregation behavior of the SMPs is demonstrated by the adhesion force tests. The reversible hydrogen bonding interactions in SE coating contribute to the self-aggregation behavior of the SMPs, which is revealed by the thixotropy test and the FTIR analysis at different temperatures. With the self-aggregation behavior, the crushed proppants can aggregate *in situ* to form a stable structure again and therefore reduce the threat of narrowing down the fracture and proppant flowback, which has an important practical significance during oil and gas production.
© 2021 The Authors. Publishing services by Elsevier B.V. on behalf of KeAi Communications Co. Ltd. This is an open access article under the CC BY-NC-ND license (http://creativecommons.org/licenses/by-nc-nd/4.0/).

1. Introduction

The primary target of hydraulic fracturing treatment is to create a highly conductive flow path to a wellbore that promotes the production potential of the well (Gillard et al., 2010; Tan et al., 2019; Wang, 2019; Yan et al., 2011; Zheng et al., 2017). However, the integrity of the propped fracture and fracture conductivity tends to be adversely impacted by proppant flowback (Guo et al., 2020; Hou et al., 2017; Mclennan et al., 2015; Wang et al., 2019). What is worse, the backproduction of proppants has a detrimental wear effect on the downhole and surface equipment, which imposes a serious threat to oil and gas production safety and multiplies the operation costs (Shaari et al., 2008; Vo et al., 2014; Wang et al., 2020).

Various physical or chemical techniques and additives have been applied to provide a limited solution to proppant flowback control (Table 1.). Forced closure is applied to close the fracture rapidly and trapping proppants in a uniform distribution, while the closure stress does not always hold proppants in place and may actually contribute to flowback (Nguyen et al., 2006). Mechanical screens installed across perforated intervals to prevent proppant flowback are known to add additional skin factors to the production, which leads to lower production rates with the same drawdown level and increase the cost of operation (Salah et al., 2016). Resin-coated proppants (RCPs) have been used during fracturing treatment to consolidate proppants since the 1980s (Norman et al., 1992). However, RCP application has been limited in the past few years due to its chemical interactions with fracturing fluids and proppant pack permeability reduction (Nguyen et al., 2013). In addition, RCPs are applicable for flowback control primarily at elevated temperatures above 60 °C; at lower temperatures, an additional activator and a long curing time may be required (Horadam et al., 2018; Letichevskiy et al., 2015). Fibers mixed with proppants is another effective way to stabilize proppant packs and have been implemented since the late 1990s (Burukhin et al., 2012). Fibers physically intertwin with the proppants to form a physical network structure to minimize proppant movement within the pack during production, and the effect of the fibers does not depend on temperature activation or time (Howard et al., 1995; Sallis et al., 2014). After construction, the fluid can flow back in a great quantity without shutting, and efficiency of fluid flowing back is significantly enhanced (Sitdikov et al., 2009). However, an additional workstage is needed to mix the fibers with the fracturing fluid

* Corresponding author.
E-mail address: zhangguicaiupc@126.com (G.-C. Zhang).

https://doi.org/10.1016/j.petsci.2021.12.025
1995-8226/© 2021 The Authors. Publishing services by Elsevier B.V. on behalf of KeAi Communications Co. Ltd. This is an open access article under the CC BY-NC-ND license (http://creativecommons.org/licenses/by-nc-nd/4.0/).

Table 1
Advantages and disadvantages of the proppant flowback control strategies.

Strategy	Advantages	Disadvantages
Forced closure (Nguyen et al., 2006)	No additives required	Limited effect
Mechanical screens (Salah et al., 2016)	No additives required	Lower production rates, additional costs
RCP	Suitable for high temperature up to 200 °C (Horadam et al., 2018)	Dependent on temperature and curing time, chemical interaction with fracturing fluids, permeability reduction (Letichevskiy et al., 2015; Nguyen et al., 2013)
Fibers	Independent on temperature and time (Howard et al., 1995; Sallis et al., 2014)	Additional workstage (Bai et al., 2019; Samuel et al., 2007)
Self-aggregating proppants	Self-aggregation (Liao et al., 2019; Lu et al., 2016)	Additional as-needed spraying device (Fu et al., 2016; Lu et al., 2018; Stegent et al., 2010)

evenly during fiber injection (Bai et al., 2019; Samuel et al., 2007). Self-aggregating proppants can realize self-aggregation by sticky coating, zeta potential alteration or strong capillary attraction to prevent proppant flowback and increase the pack porosity by hindering compaction (Liao et al., 2019; Lu et al., 2016; Weaver and Nguyen, 2010). However, the existing self-aggregating proppants tend to consolidate during the storage and transportation, and therefore they have to be prepared *in situ* with additional as-needed spraying device and result in more operating costs (Fu et al., 2016; Lu et al., 2018; Stegent et al., 2010). Despite these limitations, self-aggregating proppants have an innate advantage over traditional flowback control strategies. The traditional flowback control strategies rely on the one-off effect and they are helpless if the proppants are out of their original positions. By contrast, self-aggregating proppants can aggregate together spontaneously, and re-aggregate together if the proppant congeries are scattered to strewing sands (Treybig et al., 2016).

In the present study, the self-healing elastomer (SE) modified proppants (SMPs) are prepared for proppant flowback control. A series of SMPs' properties including basic properties, self-aggregation behavior, fracture conductivity, flowback control property, and the functional mechanism are analyzed. Superior to the existing self-aggregating proppants, the SMPs possess a firm and dry coating at room temperature, making their storage, transport and use as conventional proppants possible. The SMPs can aggregate together spontaneously through reversible hydrogen bonding interactions to prevent proppant flowback and increase the pack porosity, showing great potential in hydraulic fracturing.

2. Experimental

2.1. Materials

Dicarboxylic acid (98% purity, Huakai Chem, China) was used as received. Ethylenediamine (99% purity), *n*-butylamine (99% purity), isopropanol (99.7% purity), hydrochloric acid (HCl, 36.0%–38.0% purity), hydrofluoric acid (HF, 40% purity), tetrahydrofuran (THF, 99.8% purity) and deuterochloroform ($CDCl_3$) were purchased from Sinopharm Chemical Reagent Co., Ltd., China. Potassium chloride (KCl, 99.8% purity) and sodium carbonate (Na_2CO_3, 99.5% purity) were supplied by Aladdin Reagent Co., Ltd., USA. Ceramic proppants with a size range of 0.25–0.425 mm were taken from the Shengli Oilfield, China. Diesel was acquired from a gas station. Quartz microspheres with a grain diameter of 0.35 mm were obtained from Shili Abrasive Industry, China.

2.2. Methods

2.2.1. Synthesis and characterization of the self-healing elastomer (SE)

The synthetic process of SE is shown in Fig. 1. Equimolar mixtures of dicarboxylic acid and ethylenediamine are added and stirred in a round-bottom flask placed in an electric jacket. The reaction is conducted at 230 °C for 5–6 h. *n*-Butylamine is added to the flask as the chain terminator at the late stage of polycondensation. All the procedures are conducted with nitrogen protection.

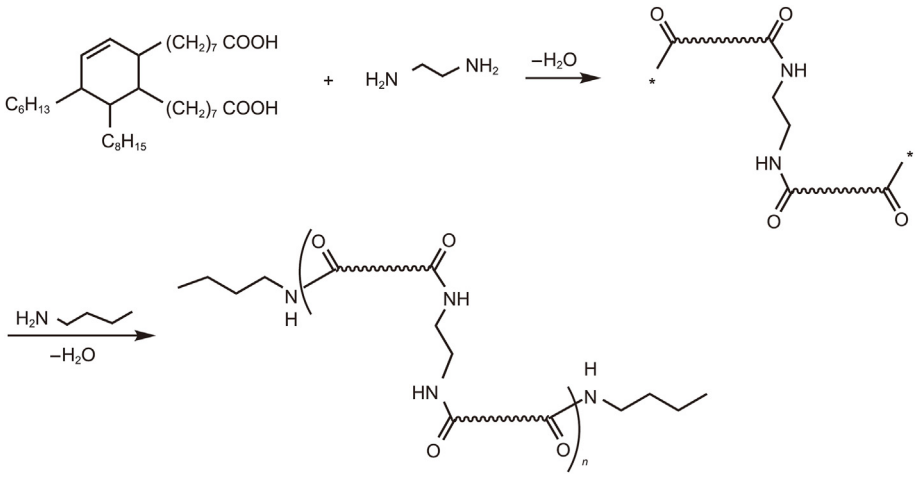


Fig. 1. Synthetic process of the SE.

The functional groups of the SE are characterized by Fourier transform infrared (FTIR) spectroscopy (ThermoFisher iS50 FTIR Spectrometer equipped with a Harrick high-temperature reaction tank) within the wavenumber range of 4000–500 cm^{-1} and the proton nuclear magnetic resonance (^1H NMR) spectra (Bruker Advance 500 MHz spectrometer) using $CDCl_3$ as a solvent. The number-average molecular weight (M_n) and the polydispersity index (PDI) of the SE are measured by gel permeation chromatography (GPC, Shimadzu GPC20A) with THF as the solvent (for SE, M_n = 6050, PDI is 1.21). Thermal characteristics of the SE are determined by thermogravimetric analysis (TGA) and differential scanning calorimetry (DSC). TGA is conducted on a NETZSCH TG 209F3 instrument under a nitrogen atmosphere with a heating rate of 10 °C/min from ambient temperature to 550 °C. The DSC measurements are carried out on a TA Instrument Q20 with a heating rate of 10 °C/min from 0 to 250 °C. Oscillatory shear tests are performed with an Anton Paar MCR92 rotational rheometer. Parallel plates with a diameter of 25 mm and a gap size of 1.0 mm are used for all tests. A fresh sample is prepared for each test for consistency. The thermomechanical property tests are applied from 50 to 220 °C under 1% shear amplitude at an angular frequency of 1 rad/s. The thixotropy test procedure consists of three intervals. The shear amplitude of each interval is set as 1%, 50% and 1%, respectively. The angular frequency is 1 rad/s during the thixotropy test procedure.

2.2.2. Self-healing elastomer modified proppant (SMP) preparation

SMPs are prepared according to the following steps. First, the surface modifier is prepared by mixing SE and isopropanol together at a mass ratio of 2:3. The isopropanol is used as solvent. Second, 40 g of the surface modifier is mixed with 1 kg of untreated proppants in a blender at a speed of 200 r/min for 5 min. Subsequently, the mixture is dried and ground at ambient temperature (25 °C) to obtain SMPs (Fig. 2a). The surface morphology of the proppants and the elemental composition are characterized by scanning electron microscopy (SEM, Hitachi SU3500) and energy dispersive spectroscopy (EDS). As presented in Fig. 2b and c, the surface of SMP is much smoother than that of the untreated proppants due to the coating. The atomic percents of the inherent elements (such as O, Al, Si) decrease significantly, whereas the carbon content improves markedly. In addition, it can be clearly observed that a new N peak is located at 0.37 eV in the EDS spectra of the SMPs, which demonstrates that the SE has effectively adsorbed onto the surface of the proppants.

2.2.3. SMP performance

The performances of the untreated proppants and the SMPs, including the bulk density, roundness, sphericity, acid solubility and compressive strength, are tested according to industry standard "Proppant performance test method for hydraulic fracturing and gravel packing operations" (SY/T5108-2014). The roundness and sphericity of the SMPs are observed using an optical microscope (XK-G600S, SINICO) and calculated by comparison with standard roundness and sphericity plates. The compressive strength tests are conducted using a universal testing machine (WDW-20KN, Weipin testing machine).

The fracture conductivity is measured by a conductivity test apparatus designed according to the industry standard "Procedures for measuring the conductivity of proppants" (SY/T 6302-2019). The fracture conductivity test apparatus is composed of a load frame, a flowmeter, a pressure gauge, a conductivity cell and several valves (Fig. 3). The proppants are placed in the conductivity cell at a concentration of 10 kg/m^2. The placement area of the conductivity cell is 64.5 cm^2. The injection fluid is 2 wt% KCl brine with a flow rate of 5 mL/min. The closure pressure is started at 6.9 MPa and increased to 13.8 MPa and then increased in 13.8 MPa steps up to 69 MPa. Every step lasts over a period of 60 min. The temperature remains 120 °C during the whole process. The median pressure and pressure drop across the conductivity cell are measured at different closure stress and the fracture conductivity is calculated.

The maximum sand free rate (MSFR) is employed to evaluate the proppant flowback control behavior. The proppants are placed in the conductivity cell, and the closure pressure is imposed. The

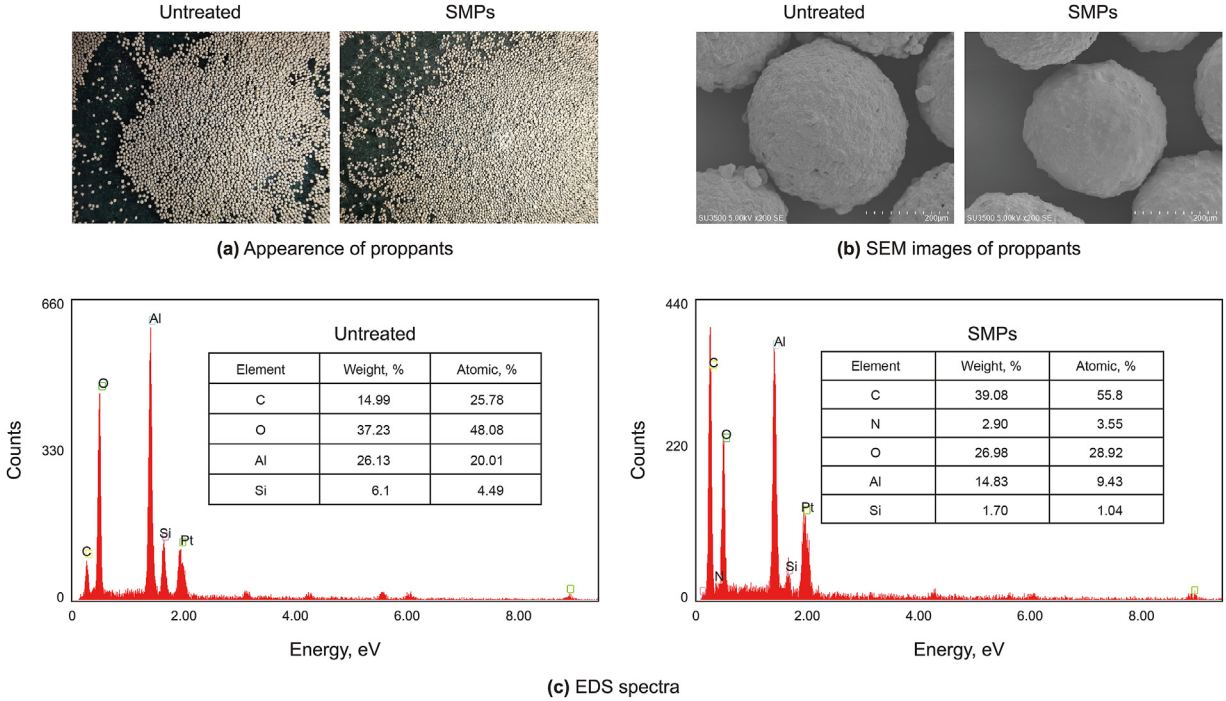


Fig. 2. Surface characterization of the untreated proppants and SMPs.



Fig. 3. Fracture conductivity test apparatus.

proppant pack is saturated with the injection fluid and aged for 24 h and then displaced with 2 wt% KCl brine. The initial flow rate is set as 5 mL/min and increased to 10 mL/min and then increased in 10 mL/min steps up to 200 mL/min. The flow rate is recorded as the MSFR when the proppants are found in the effluent. All the tests are conducted at 120 °C.

2.2.4. Adhesion force test

An adhesion force testing apparatus (Fig. 4) is set up to quantitatively characterize the self-aggregation ability and the influence of temperature on consolidation strength of the SMPs. It should be noted that the adhesion force between the SMPs is very small (only dozens of millinewtons at most). Considering that the results of the adhesion force test are quite influenced by the regularity of the particles, hence, regular-shaped self-healing elastomer modified quartz microspheres are optimized to simulate the SMPs to reduce the experimental error. The particle size of the untreated quartz microspheres is similar to the untreated proppants. Meanwhile, the preparation process of the self-healing elastomer modified quartz microspheres is exactly the same as the SMPs. Adhesion force tests are conducted using the following procedure. (1) The self-healing elastomer modified quartz microspheres are fixed at the bottom of the pressure transducer and the tip of the probe separately. (2) The pressure transducer and the probe are immersed in water and adjust to move toward each other. The reading of the pressure transducer is set to zero when slight contact is established between the quartz microspheres. (3) After resting for 6 h, the quartz microspheres are separated with a fairly low velocity (0.1 mm/s). (4) Record the interaction force history between quartz microspheres. The peak force is considered as the adhesion force between the self-healing elastomer modified quartz microspheres.

3. Results and discussion

3.1. Characterization of the SE

3.1.1. Structural characterization

Fig. 5 shows the infrared spectrum of the SE. CH_3 and CH_2 stretching vibrations and bending vibrations are observed at 2919, 2850, 1455, and 1376 cm^{-1}, respectively. The ν(N—H) is observed at 3288 cm^{-1}. A strong absorption peak at 1636 cm^{-1} is attributed to ν(C═O). β(N—H) produces a strong absorption peak at 1555 cm^{-1}. The absorption peak at 722 cm^{-1} is attributed to $(CH_2)_n$ ($n \geq 4$). Fig. 6 displays the ^1H NMR spectrum of the SE. The methylene ^1H signal of ethylene is detected at $\delta = 2.20$ (CH_2—CONH—), and the ^1H signals of the amide group and the free amino group are detected at $\delta = 6.79$–6.93 (CONH) and $\delta = 3.69$ ($-NH_2$), respectively. The infrared spectrum and ^1H NMR spectrum confirm that the SE was rich in carbonyl and amide groups, which contributes to the formation of hydrogen-bonds.

3.1.2. Thermal characterization

The thermal behavior of the SE coating is revealed in Fig. 7. As demonstrated by the typical TGA thermograms, the SE is thermally stable up to approximately 350 °C. A dramatic loss in weight occurs between 370 and 480 °C because of the decomposition of SE. The tested sample has completely degraded at approximately 500 °C. According to the DSC curve, the glass transition temperature (T_g) of the SE is 47.7 °C, indicating that the SE is glassy at room temperature, which makes the SMPs possess a firm and dry coating. The glass-rubber transition at T_g results from the onset of long-range coordinated molecular motion of the SE as the temperature increases (Sperling, 2006). The molecular motion of the SE keeps increasing with the temperature. The melting temperature T_m is taken at 207.2 °C, at which the SE behaves as a viscous liquid due to

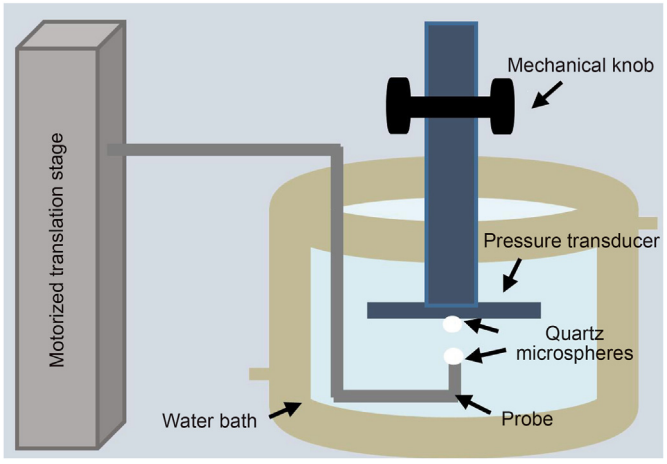


Fig. 4. Schematic of adhesion force testing apparatus.

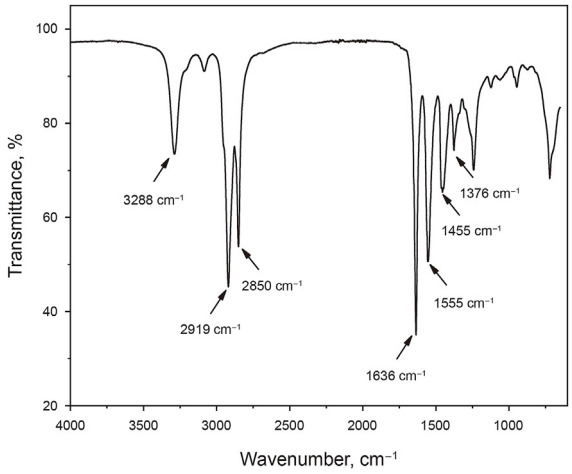


Fig. 5. Infrared spectrum of the SE.

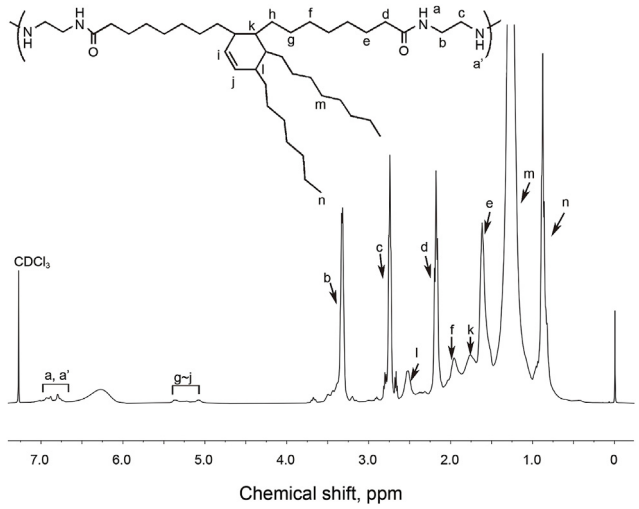


Fig. 6. ^{1}H NMR spectrum of the SE.

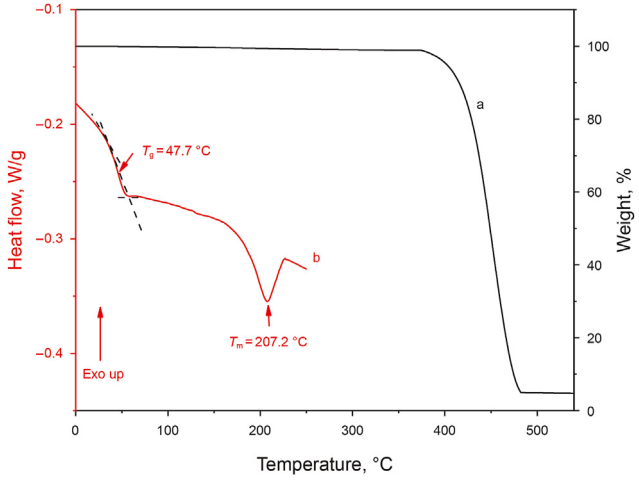


Fig. 7. TGA (a) and DSC (b) curves of the SE.

the accelerated molecular motion and reduced chain entanglement (Sperling, 2006). The liquid SE coating at T_m becomes completely invalidated due to the structural strength failure.

The thermomechanical behavior of the SE above T_g is disclosed by Fig. 8. The SE exhibits rubberlike viscoelasticity and possesses a certain structural strength at 50 °C. The storage modulus (G') and the loss modulus (G'') are as high as 5.5×10^4 Pa and 6.2×10^4 Pa, respectively. As the temperature continues to increase, G' and G'' decrease drastically due to the disentanglements of molecule chains, which is supported by the endothermic process observed by DSC (Chen et al., 2013). The G' and G'' dip below 100 Pa at 200 °C, which are less than 1% of the initial values at 50 °C, indicating that the structural strength of the SE almost destroyed.

3.2. Performances of SMPs and untreated proppants

3.2.1. Basic properties

The basic properties of the SMP are further tested. As exhibited in Table 2, the bulk density of the SMPs is lower than that of the untreated proppants, which endows the SMPs with better suspension and transportation in the fracturing fluid and fractures. Both the roundness and sphericity of the SMPs meet the standard

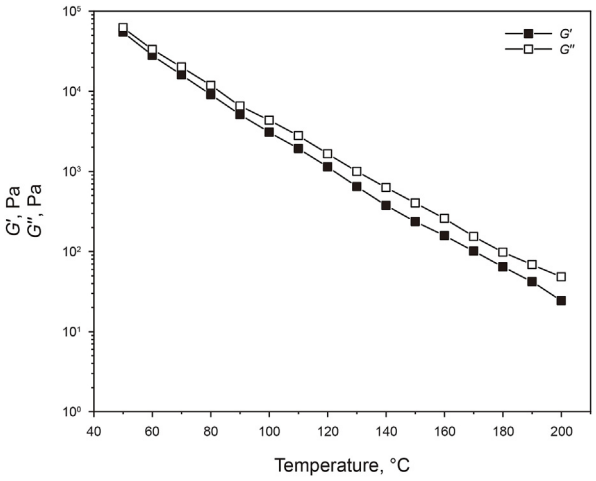


Fig. 8. Thermomechanical behavior of SE from 50 to 200 °C.

requirements. The acid solubility of the SMPs exceeds the permitted level slightly due to the chemical reaction of the SE coating with the mixed acid solution. Table 2 also shows the maximum compressive strength when the crushing rate is less than 10%. Although the compressive strength of the SMPs is slightly lower than that of the untreated proppants due to the brittle coating, the fracture conductivity of the SMPs is barely impacted at a high closure pressure. The proposed reason for this phenomenon is explain in detail in later section. To sum up, the properties of SMPs are basically comply with the criteria of the standard and are eligible for engineering application.

3.2.2. Self-aggregation behavior of the SMPs

The self-aggregation behavior refers to that the SMPs can aggregate together spontaneously, and reaggregate together if the proppant congeries are scattered to strewing sands. Adhesion force tests are conducted to quantitatively characterize the influence of temperature on self-aggregation behavior of the SMPs. As mentioned above, the self-healing elastomer modified quartz microspheres are optimized to simulate the SMPs to reduce the experimental error. According to the interaction force history during the separating process (Fig. 9), the adhesion force between the quartz microspheres shows a trend from rising to decline with the increasing temperature. Given that the T_g of the SE coating is 47.7 °C, the adhesion force at 25 °C is extremely weak (5 mN) since the intermolecular motions of the SE coating has been largely restricted in the glassy state (Chen et al., 2013). The glassy coating enables the SMPs to be stored, transported and used as conventional proppants possible. As the temperature increases to 50 °C, the viscoelasticity of the SE coating contributes to the sharp increase in the adhesion force (73 mN). However, according to the thermomechanical property test above T_g, the G' and G'' of the SE coating decrease drastically with the temperature, which will reduce the structural strength and the adhesiveness of the SE coating between the quartz microspheres. Hence, an evident decline in the adhesion force occurs as the temperature increases to 90 °C. The adhesion force at 90 °C (35 mN) is only half of that at 50 °C. Although the adhesion force tests at higher temperature cannot be proceeded subject to the instrument, the self-aggregation of SMPs and the further reduction of adhesion force with the increasing temperature are predictable.

To further prove the re-aggregation behavior of the SMPs, the continuous contact-separation test between the self-healing elastomer modified quartz microspheres is operated at 50 °C. The

Table 2
Basic properties of SMPs and untreated proppants.

Items	Bulk density, g/cm^3	Roundness	Sphericity	Acid solubility, %	Compressive strength, MPa
Untreated proppants	1.57	0.9	0.9	3.5	48
SMPs	1.36	0.8	0.8	5.1	41
Standard requirements	–	> 0.7	> 0.7	< 5	> 35

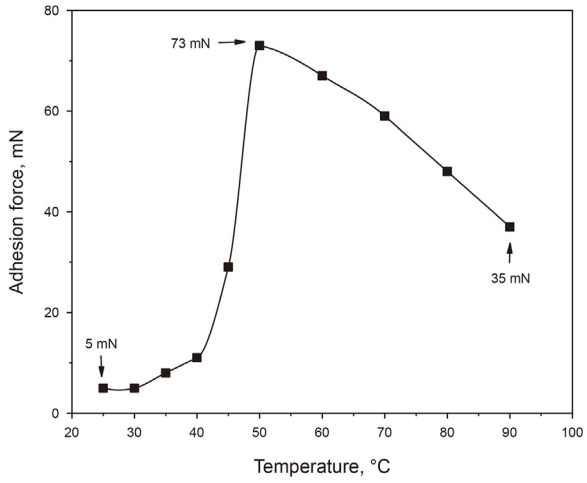


Fig. 9. Relationship of the adhesion force with the temperature.

quartz microspheres are operated to keep in contact for 6 h and then separated with each other. Repeat this contact-separation process for 20 times and record the adhesion force in every cycle. Fig. 10 illuminates that there is an obvious decline in the adhesion force in the first few cycles, which might be resulted from the uneven distribution of the SE coating during the separation process, and then the adhesion force hardly changes during the subsequent contact-separation processes. The adhesion force is 85.1% of the original force after being contacted and separated 20 times and then remains almost constant, demonstrating that the SMPs can re-aggregate together if the proppants congeries are scattered to strewing sands.

3.2.3. Fracture conductivity

The conductivity of the proppant pack is evaluated by a conductivity test instrument. To minimize experimental error, each test has been conducted in triplicate. It should be noted that the SMPs exhibit a significantly higher conductivity than the untreated proppants throughout the test (Fig. 11), although the conductivities of both proppant packs decrease drastically with the increasing closure pressure due to compaction and fragment blockage. At a low closure pressure (<40 MPa, lower than the compressive strength), the decrease in the fracture width leads to a conductivity reduction. However, the SMPs tend to form aggregates with a certain strength to hold the fracture, which contributes to the fracture conductivity maintenance. At a high closure pressure (>50 MPa, higher than the compressive strength), the fracture conductivity continues to decline due to the continuous reduction in the fracture width and the permeability reduction caused by the blockage of the proppant fragments. In terms of untreated proppants, the migration of the broken proppant fragments will plug the pores, leading to a drastic conductivity decrease. In contrast, the released SMP fragments will adsorb and anchor on the modified proppant surface again due to the self-aggregating property, which will reduce the risk of blockage of the flow channels. Fig. 12 illustrates the crushed proppant pack and the morphology of the crushed proppants. As shown in Fig. 12a, all of the fragments of the untreated proppants are scattered and are prone to migration with the formation fluids. By contrast, the broken SMPs are still consolidated, and the fragments are aggregate together (Fig. 12b). It can be concluded that the self-aggregation behavior of the SMPs enables the crushed proppants to aggregate *in situ* to form a stable structure again and thus effectively reduces the threat of fracture conductivity reduction.

3.2.4. Flowback control behavior

The flowback control property of SMPs and untreated proppants as well as their compatibility with injection fluids with different characteristics are evaluated by using the MSFR as an indicator. KCl brine, HCl solution, Na_2CO_3 solution and diesel are recommended as injection fluids for saturation. Considering that the MSFR refers to the maximum injection rate when the particles start to be

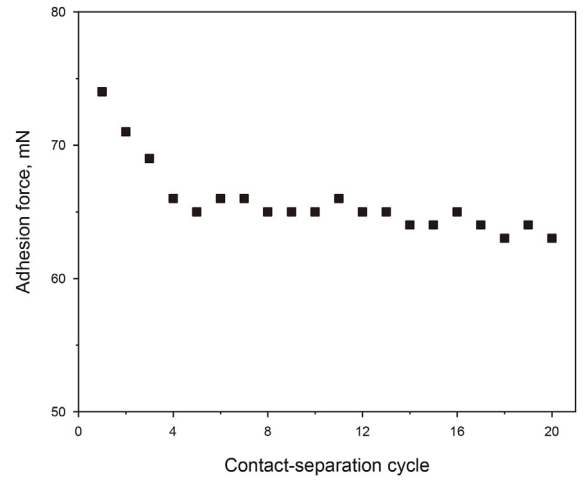


Fig. 10. Adhesion force change during continuous contact-separation cycles at 50 °C.

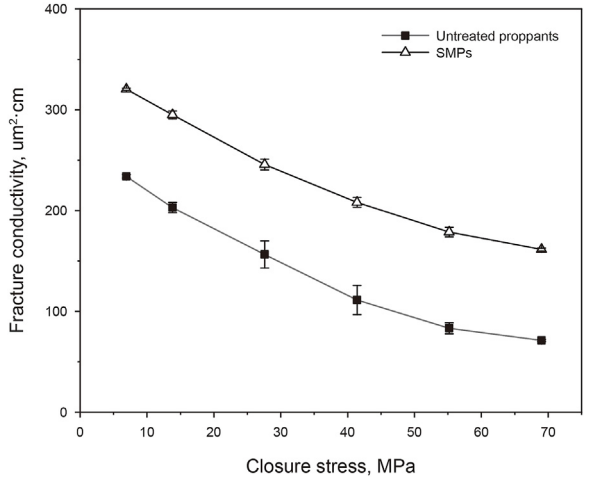


Fig. 11. Fracture conductivity of the proppant packs with different closure pressures.

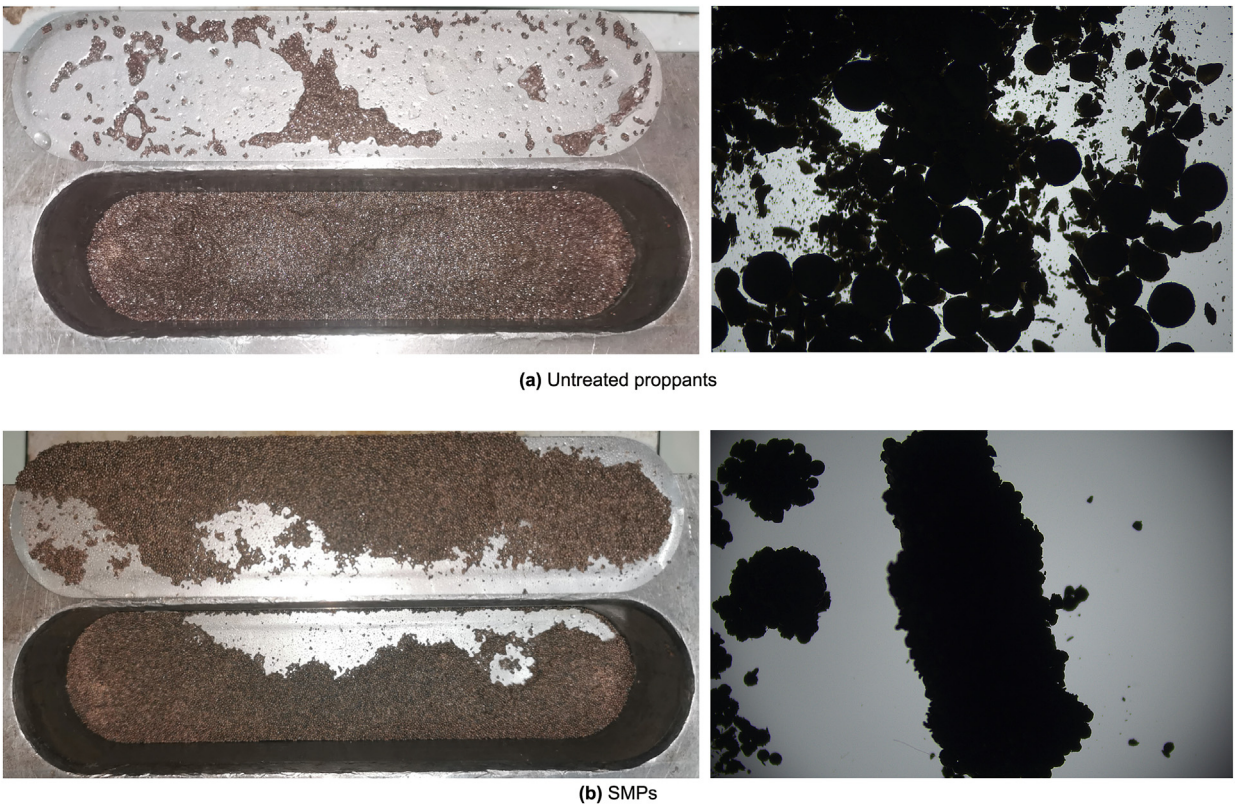


Fig. 12. Crushed proppant pack and the morphology of crushed proppants.

flushed out from the production end, the proppant flowback rate is inversely proportional to the MSFR. MSFR under different closure pressures is displayed in Fig. 13. For both types of proppants, the higher the closure pressure is, the better the proppant flowback control ability. It is noteworthy that, the MSFR of SMPs is almost treble the untreated proppants when the proppant pack is saturated with 2 wt% KCl brine. The growth in MSFR is resulted from the self-aggregation behavior of SMPs. Different from the SMPs, the injection fluids have a negligible influence on the untreated proppants. The SMPs incorporate preferable alkali tolerance since the MSFR barely changes after being treated with 5 wt% Na_2CO_3 solution. A similar situation occurs when the proppant pack is saturated with diesel. High-salinity (10 wt%) KCl brine exhibits a slight adverse impact on aggregation strength. This might be because of the weakened molecular chain entanglement between SE coatings in high-salinity brine. As depicted in Fig. 13, the flowback control of the SMPs fails when exposed to the 5 wt%. HCl solution. Desorption occurs when the SE coating reacts with acid so that the aggregated SMPs collapse and act as untreated proppants. In summary, the flowback control property of SMPs is remarkably superior to the untreated proppants, showing great potential in proppant flowback control.

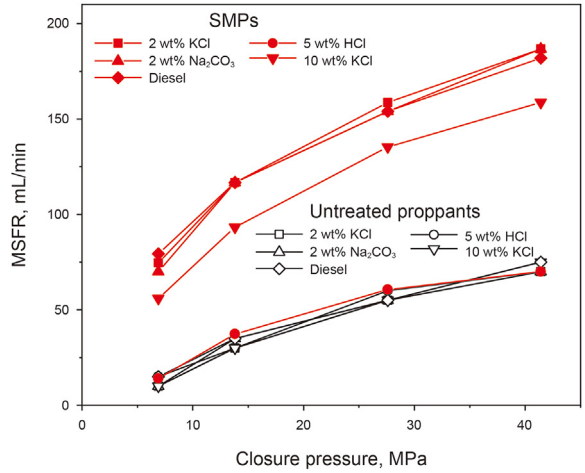


Fig. 13. MSFR changes with different injection fluids and closure pressure.

3.3. Mechanism of the self-aggregation behavior of the SMPs

Considering that the self-aggregation behavior of the SMPs is inherited from the SE coating. The reversible restoration process of the adhesion force of SMPs might be interpreted by the thixotropy of the SE coating. Thixotropic behavior means reduction of the initial structural strength when performing a high-shear process, followed by more or less rapid but complete structural regeneration in the subsequent period of rest (Fakirov, 2005). As presented in Fig. 14, the thixotropic behavior of the SE at different temperatures consist of three intervals. Take 50 °C for example. The G' of the SE remains on a constant plateau value (5.5×10^4 Pa) at low-shear interval (I, amplitude = 1%) in the period of 0–100 s. Here, the low-shear condition is adopted to simulate the state-at-rest of the SE coating and SMPs. Then G' shows a drastically reduction in the high-shear interval (II, amplitude = 50%) in the period of 100–300 s, indicating that the internal structure of the SE has been partially broken. The high-shear interval is used to simulate the high-shear conditions occurring during an application process, when the SMPs are scattered due to the formation stress changes. Then the same shear conditions as in the interval I is imposed on

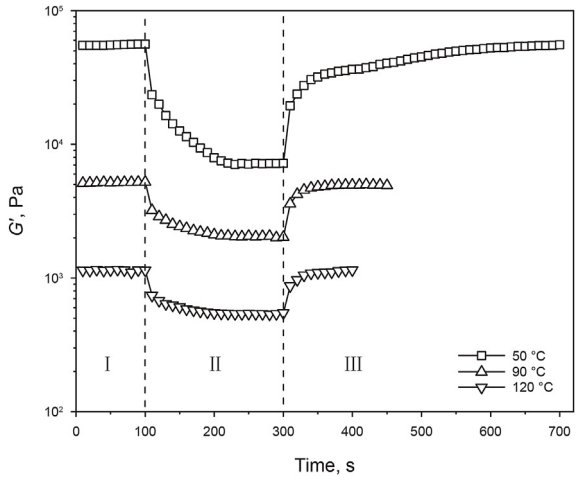


Fig. 14. Thixotropic behavior of the SE.

the SE sample to facilitate the regeneration interval (III, amplitude = 1%). The G' rises up to 5.4×10^4 Pa and keeps almost constant, with a value very similar to that in interval I, indicating that the structure strength of the SE almost restored. The regeneration interval indicates that the scattered SMPs can adapt to the changing reservoir conditions and re-aggregate with the restore process of the SE coating. A similar phenomenon occurs at 90 and 120 °C. The thixotropy test verifies the self-healing behavior of the SE coating, indicating that the SMPs can aggregate together spontaneously and can re-aggregate together if the proppants congeries are scattered to strewing sands.

In view of the SE coating is rich in amidogens and carbonyl groups, the self-healing process of the SE coating and the concomitant self-aggregation process of SMPs might be resulted from the reversible hydrogen-bonding interactions of the SE coating between the amidogens and carbonyl groups. The FTIR of the SE coating under variable temperatures are conducted to test this hypothesis. Fig. 15 shows the absorption strength changes and wavenumber shifts of N–H and C=O during the heating and cooling process. The frequency of ν(N–H) shifts from 3284 to 3307 cm^{-1} when the temperature increases from 20 to 180 °C (Fig. 15a). In addition, during the heating process, the frequency of ν(C=O) shifts toward higher wavenumbers, whereas the β(N–H) signals shifts toward lower wavenumbers. This phenomenon is reversed during the cooling process. The frequency of ν(N–H) shifts from 3307 back to 3288 cm^{-1} when the temperature decreases from 180 to 20 °C (Fig. 15b). The frequency of ν(C=O) shifts back toward lower wavenumbers, and the β(N–H) signals shifts back toward higher wavenumbers. The FTIR spectra during the heating and cooling process confirm that the reversible hydrogen bonding interactions do exist in the SE coating. Hydrogen bonds in SE coating are apt to reform when they are broken by external force, which endows the SMPs with the self-aggregation behavior (Kajita et al., 2017). When the aggregated SMPs are departed by external force, the free N–H and C=O on the adjacent SMPs interface can readily form bridges via hydrogen bonds across the interface and will help the re-aggregation behavior occur (Li et al., 2021).

4. Conclusions

We proposed a self-healing elastomer modified proppants for proppant flowback control in hydraulic fracturing. The self-healing elastomer was synthesized through polymerization and characterized by Fourier transform infrared spectroscopy as well as the proton nuclear magnetic resonance. Thermal properties of the self-healing elastomer were revealed by the thermogravimetric analysis and the differential scanning calorimetry. The thermomechanical property and thixotropy of the self-healing elastomer were evaluated by rheological tests. The basic performance, fracture conductivity and flowback control properties of the self-healing elastomer modified proppants were evaluated through laboratory experiments. Adhesion force tests were conducted to characterize the aggregation property of the self-healing elastomer modified proppants. The results indicate that:

(1) The self-healing elastomer modified proppants have a firm and dry coating at room temperature, making their storage, transport and use as conventional proppants possible.
(2) The self-healing elastomer modified proppants incorporates admirable self-aggregation behavior. As a result, the fracture conductivity and the flowback control property of the self-healing elastomer modified proppants is remarkably superior to the untreated proppants.
(3) The reversible hydrogen bonding interactions contribute to the self-aggregation and re-aggregation process of the self-healing elastomer modified proppants.

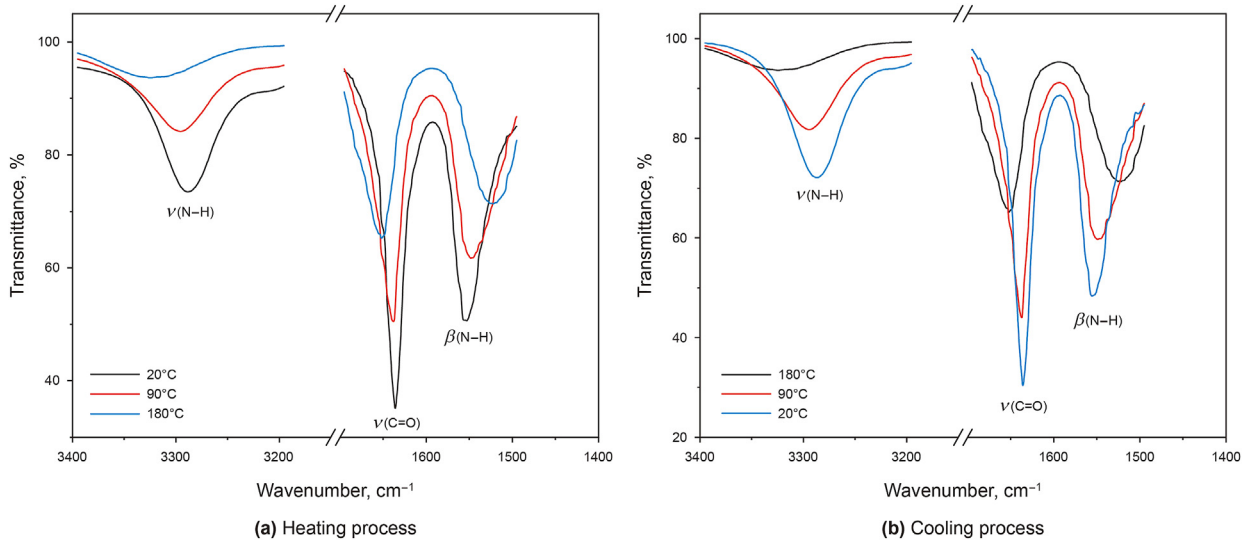


Fig. 15. FTIR spectra of the SE coating during the heating and cooling process.

Availability of data and material

All data generated or analyzed during this study are included in this manuscript.

Code availability

Not applicable.

Declaration of competing interest

The manuscript was written through contributions of all authors. All authors have given approval to the final version of the manuscript.

We declare that we do not have any commercial or associative interest that represents a conflict of interest in connection with the work submitted.

Acknowledgments

The authors gratefully appreciate the support from the National Key R&D Program of China (grant number 2018YFA0702400), the Major Scientific and Technological Projects of CNPC (grant number ZD2019-183-007) and the Fundamental Research Funds for the Central Universities (grant number No. 19CX02017A).

References

Bai, M.W., Wang, Y.H., 2019. Technology and experimental research of fracturing fluid fiber mixing device. Petrochem. Equip. 22, 9–13 (in Chinese).

Burukhin, A., Kalinin, S., Abbott, J., Bulova, M., 2012. Novel interconnected bonded structure enhances proppant flowback control. In: SPE International Symposium and Exhibition on Formation Damage Control. https://doi.org/10.2118/151861-MS.

Chen, Y.J., Wu, W., Himmel, T., Wagner, M.H., 2013. Structure and rheological behavior of thermoreversible supramolecular polymers with weak multiple hydrogen bonds. Macromol. Mater. Eng. 298, 876–887. https://doi.org/10.1002/mame.201200139.

Fakirov, S., 2005. Handbook of Condensation Thermoplastic Elastomers. Wiley-VCH Verlag GmbH & Co. KGaA, Weinheim.

Fu, L.P., Zhang, G.C., Ge, J.J., Liao, K.L., Jiang, P., Pei, H.H., Li, X.Q., 2016. Surface modified proppants used for porppant flowback control in hydraulic fracturing. Colloids Surf. A Physicochem. Eng. Asp. 507, 18–25. https://doi.org/10.1016/j.colsurfa.2016.07.039.

Gillard, M., Medvedev, O., Peña, A., Medvedev, A., Peñacorada, F., d'Huteau, E., 2010. A new approach to generating fracture conductivity. In: SPE Annual Technical Conference and Exhibition. https://doi.org/10.2118/135034-MS.

Guo, J.C., Yang, R.Y., Zhang, T., Lu, Q.L., Mu, K.F., 2020. Experimental and numerical investigations of proppant pack effect on fracture conductivity of channel fracturing. Energy Sci. Eng. 8, 3995. https://doi.org/10.1002/ese3.791, 401.

Horadam, W., Venkat, N., Tran, T., Bai, L.T., Josyula, K., Mehta, V., 2018. Leaching studies on Novolac resin-coated proppants-performance, stability, product safety, and environmental health considerations. J. Appl. Polym. Sci. 135, 45845. https://doi.org/10.1002/app.45845.

Hou, T.F., Zhang, S.C., Ma, X.F., Shao, J.J., He, Y.A., Lv, X.R., Han, J.Y., 2017. Experimental and theoretical study of fracture conductivity with heterogeneous proppant placement. J. Nat. Gas Sci. Eng. 37, 449–461. https://doi.org/10.1016/j.jngse.2016.11.059.

Howard, P.R., King, M.T., Morris, M., Feraud, J.-P., Slusher, G., Lipari, S., 1995. Fiber/proppant mixtures control proppant flowback in South Texas. In: SPE Annual Technical Conference and Exhibition. https://doi.org/10.2118/30495-MS.

Kajita, T., Noro, A., Matsushita, Y., 2017. Design and properties of supramolecular elastomers. Polymer 128, 297–310. https://doi.org/10.1016/j.polymer.2017.03.010.

Letichevskiy, A., Parfenov, A., Belyakova, L., Konchenko, A., Borisenko, A., Parkhonyuk, S., Olennikova, O., Klyubin, A., 2015. Proppant flow back control for fracturing low temperature formations of Russia methodology and case studies. In: SPE Russian Petroleum Technology Conference. https://doi.org/10.2118/176650-MS.

Li, J.D., Zhang, G.C., Ge, J.J., Jiang, P., Pei, H.H., Qiao, W.L., 2021. Sand consolidation system based on hydrogen-bonding self-healing resin. J. China Univ. Pet., Ed. Nat. Sci. 45, 137–143. https://doi.org/10.3969/j.issn.1673-5005.2021.01.016.

Liao, K.L., Ge, J.J., Fu, L.P., Li, J.D., Li, T.L., Zhang, G.C., 2019. Study of novel self-initiated aggregating proppant for channel fracturing. Int. J. Oil Gas Coal Technol. 20, 327–341. https://doi.org/10.1504/IJOGCT.2019.098464.

Lu, W.B., O'Neil, B., Zhang, K.W., Wang, C.Z., Quintero, H., 2016. Enhancing proppant flowback control through surface treatment of proppant. In: SPE International Petroleum Technology Conference. https://doi.org/10.2523/IPTC-18796-MS.

Lu, W.B., O'Neil, B., Zhang, K.W., Wang, C.Z., Quintero, H., 2018. Mitigating proppant flowback through surface treatment of proppant-laboratory studies and field performance. In: SPE International Hydraulic Fracturing Technology Conference and Exhibition. https://doi.org/10.2118/191438-18IHFT-MS.

Mclennan, J., Walton, I., Moore, J., Brinton, D., Lund, J., 2015. Proppant backflow: mechanical and flow considerations. Geothermics 57, 224–237. https://doi.org/10.1016/j.geothermics.2015.06.006.

Nguyen, P.D., Rickman, R.D., Weaver, J.D., Vonk, T.Z., Loghry, R.A., 2013. New Treatment Method for Enhancing Propped Fracture Conductivity: a Laboratory Study. SPE European Formation Damage Conference & Exhibition. https://doi.org/10.2118/165173-MS.

Nguyen, P.D., Stegent, N.A., Ingram, S.R., 2006. Remediation of production loss due to proppant flowback in existing wellbores. In: SPE Annual Technical Conference and Exhibition. https://doi.org/10.2118/102629-MS.

Norman, L.R., Terraelna, J.M., McCabe, M.A., Nguyen, P.D., 1992. Application of curable resin-coated proppants. SPE Prod. Oper. 7, 43. https://doi.org/10.2118/20640-PA, 349.

National Energy Administration, 2014. SY/T5108-2014 Proppant Performance Test Method for Hydraulic Fracturing and Gravel Packing Operations. Petroleum Industry Press, Beijing (in Chinese).

National Energy Administration, 2019. SY/T 6302-2019 Procedures for Measuring the Conductivity of Proppants. Petroleum Industry Press, Beijing (in Chinese).

Salah, M., Abdel-Meguid, A., Abdel-Baky, A., El-Maghraby, O., 2016. A newly developed aqueous-based consolidation resin controls proppant flowback and aids in maintaining production rates in fracture-stimulated wells. In: SPE Annual Technical Conference and Exhibition. https://doi.org/10.2118/181297-MS.

Sallis, J.N., Agee, D.M., Artola, P.D., Guimaraes, C., Chaloupka, V., 2014. Proppant flowback prevention with next generation fiber technology: implementation of an innovative solution for HPHT hydraulic fracturing in Indonesia. In: SPE International Petroleum Technology Conference. https://doi.org/10.2523/IPTC-17979-MS.

Samuel, M.M., Obianwu, C.W., Chao, G., Samuel, El, Hafee, Alim, Hashim, F., Rohaya, D., 2007. An engineered fiber for the fracturing of unconsolidated sand in highly deviated wells in the Tali field of Brunei. In: SPE European Formation Damage Conference. https://doi.org/10.2118/108011-MS.

Shaari, N.E.L., Swint, A., Kalfayan, L.J., 2008. Utilizing Organosilane with hydraulic fracturing treatments to minimize fines migration into the proppant pack- a field application. In: SPE Western Regional and Pacific Section AAPG Joint Meeting. https://doi.org/10.2118/114220-MS.

Sitdikov, S.S., Serdyuk, A., Nikitin, A., Yudin, A.V., Mullen, K., Oussoltsev, D., Butula, K.K., 2009. Fiber-laden fluid: applied solution for addressing multiple challenges of hydraulic fracturing in western Siberia. In: SPE Hydraulic Fracturing Technology Conference. https://doi.org/10.2118/119825-MS.

Sperling, L.H., 2006. Introduction to Physical Polymer Science, fourth ed. John Wiley & Sons, New Jersey.

Stegent, N.A., Wagner, A.L., Montes, M., Omsberg, A., Riley, K.M., 2010. SMA technology extends the useful range of nonceramic proppants in the Eagle Ford Shale. In: SPE Tight Gas Completions Conference. https://doi.org/10.2118/136801-MS.

Tan, P., Jin, Y., Yuan, L., Xiong, Z.Y., Hou, B., Chen, M., Wan, L.M., 2019. Understanding hydraulic fracture propagation behavior in tight sandstone–coal interbedded formations an experimental investigation. Petrol. Sci. 16, 148–160. https://doi.org/10.1007/s12182-018-0297-z.

Treybig, D.S., Saini, R., Vigderman, L., Smith, K., Gray, B., Strobe, J., 2016. Consolidating sand with new generation zeta potential altering systems. In: SPE International Conference and Exhibition on Formation Damage Control. https://doi.org/10.2118/179022-MS.

Vo, L.K., Nguyen, P.D., Ling, F., Parton, C., 2014. Enhancing proppant pack conductivity with consolidation and agglomeration performance: a laboratory study. In: SPE International Symposium and Exhibition on Formation Damage Control. https://doi.org/10.2118/168188-MS.

Wang, H.Y., 2019. Hydraulic fracture propagation in naturally fractured reservoirs: complex fracture or fracture networks. J. Petrol. Sci. Eng. 38, 102911. https://doi.org/10.1016/j.jngse.2019.102911.

Wang, J., Huang, Y.X., Zhou, F.J., Liang, X.Y., 2020. The influence of proppant breakage, embedding, and particle migration on fracture conductivity. J. Petrol. Sci. Eng. 193, 107385. https://doi.org/10.1016/j.petrol.2020.107385.

Wang, S.B., Chen, F.H., Guo, J.X., Li, Y., Zhao, F., Zhou, S.Y., 2019. Adsorption damage of hydroxypropyl guar gum to porous media composed of quartz. J. Petrol. Sci. Eng. 182, 106379. https://doi.org/10.1016/j.petrol.2019.106379.

Weaver, J.D., Nguyen, P.D., 2010. Hydrophobic filming reduces Frac gel and mineral scale damage. SPE Eastern Regional Meeting, doi:10.2118/138314-MS.

Yan, T., Li, W., Bi, X.L., 2011. An experimental study of fracture initiation mechanisms during hydraulic fracturing. Petrol. Sci. 8, 87–92. https://doi.org/10.1007/s12182-011-0119-z.

Zheng, X.J., Chen, M., Hou, B., Ye, Z.H., Wang, W., Yin, C.B., Chen, X.Y., 2017. Effect of proppant distribution pattern on fracture conductivity and permeability in channel fracturing. J. Petrol. Sci. Eng. 149, 98–106. https://doi.org/10.1016/j.petrol.2016.10.023.